Comput. Methods Appl. Mech. Engrg. 201–204 (2012) 82–90

Contents lists available at SciVerse ScienceDirect

Comput. Methods Appl. Mech. Engrg.

journal homepage: www.elsevier.com/locate/cma

# On 3-D coupled BEM–FEM simulation of nonlinear electro-elastostatics

D.K. Vu, P. Steinmann *

*Chair of Applied Mechanics, University of Erlangen-Nuremberg, Egerlandstrasse 5, 91058 Erlangen, Germany*

ARTICLE INFO

*Article history:*
Received 28 April 2011
Received in revised form 24 August 2011
Accepted 25 August 2011
Available online 16 September 2011

*Keywords:*
Nonlinear electrostatics
Nonlinear elastostatics
Nonlinear coupling
Coupled BEM–FEM analysis

ABSTRACT

In this work the numerical simulation of nonlinear electro-elastostatics is considered with a special focus on the influence of the free space surrounding an electro-sensitive body. The influence of the free space on the electric field and on the deformation field inside an electro-sensitive body can become highly important for many materials and can change profoundly the simulation results. In order to take into account this influence, the free space must be simulated by using, for example, the finite element method (FEM) or the boundary element method (BEM). A coupled BEM–FEM approach is employed here to exploit the advantage of the finite element method in solving nonlinear problems and the advantage of the boundary element method in dealing with infinite domains. Numerical studies using this approach show that for materials with low electric permittivity, the free space can have a huge impact on the simulated electric and deformation fields. The same observation is expected for the general case of nonlinear electro-elasticity and nonlinear electro-viscoelasticity and constitutes the direction for future works.



## 1. Introduction

The numerical simulation of the interaction between electric fields and matter is of special interest in developing artificial muscles that are made of emerging materials like electronic electroactive polymers (EEAPs) [1–8]. Unlike the simulation of piezoelectric materials under electric stimulations, in which the electric field in the free space surrounding a material body can be in many cases considered as of minor importance and can be conveniently ignored, in dealing with EEAPs, besides the nonlinear electromechanical coupling [9], the contribution of the free space may become significant and should be taken into account [10]. This is mainly because the electric polarization of most EEAPs is quite weak. The electric permittivity of many EEAPs is approximately of one order higher than that of vacuum, see e.g. [11,12], whereas for piezoelectric materials this number is three orders higher. When the contribution of the free space is important, the simulation of EEAPs using the finite element method becomes quite cumbersome. A large finite element mesh is normally required to capture the correct response of the system (deformable body and free space). Besides, for the case of large deformation, this mesh must be updated after every few iterations. In order to overcome this difficulty, we use here the finite element method in combination with the boundary element method. The finite element method is used to model the nonlinear electroelastic body and the boundary element method is used to model the surrounding finite or infinite free space. In what follows we consider the problem of finding the deformed state of a polarizable elastic body subjected to an external electric field. We restrict ourself to the case where the electric field is static with no current and no magnetic field. The material behavior is assumed to be hyperelastic and the deformation process is assumed to be static. With these restrictions, our problem can be formulated using the theories of nonlinear elastostatics and nonlinear electrostatics. In the next sections, a brief review of nonlinear elastostatics and nonlinear electro-elastostatics is presented. For detailed formulations of nonlinear electro-elasticity, see for example [13–16].

## 2. Governing equations of nonlinear elastostatics

Let us consider a body made of elastic material. The original or undeformed configuration of the body is denoted by $\mathcal{B}_0$. In this configuration the position of a point $P$ is denoted by $\boldsymbol{X}$. Under the application of external forces (surface and volume forces), the body deforms and its deformed configuration is denoted by $\mathcal{B}_t$. The position of the point $P$ in the deformed configuration $\mathcal{B}_t$ is now denoted by $\boldsymbol{x}$, which is a function of $\boldsymbol{X}$ in the format $\boldsymbol{x} = \boldsymbol{\varphi}(\boldsymbol{X})$. Here the deformation map $\boldsymbol{\varphi}$ maps the point $P$ from the undeformed configuration $\mathcal{B}_0$ to the deformed configuration $\mathcal{B}_t$. The deformation of the body at every point inside the body is characterized by the deformation gradient $\boldsymbol{F}$, which is defined as $\boldsymbol{F} = \nabla_{\boldsymbol{X}}\boldsymbol{\varphi}$. In reference to the deformed configuration $\mathcal{B}_t$, the Cauchy stress tensor is denoted by $\boldsymbol{\sigma}$ and the equilibrium equation or quasi-static version of the balance equation of linear momentum is

$$\nabla_{\boldsymbol{x}} \cdot \boldsymbol{\sigma}^t + \boldsymbol{b}_t = \boldsymbol{0}, \tag{1}$$

* Corresponding author.
*E-mail address:* paul.steinmann@ltm.uni-erlangen.de (P. Steinmann).

0045-7825/$ - see front matter © 2011 Elsevier B.V. All rights reserved.
doi:10.1016/j.cma.2011.08.024

where $\boldsymbol{\sigma}^t$ is the transpose of $\boldsymbol{\sigma}$ and $\boldsymbol{b}_t$ is used to denote the mechanical body force (gravitational force, for example). The balance equation of linear momentum must be satisfied for all points inside $\mathcal{B}_t$. In addition to the balance equation of linear momentum, the Cauchy stress tensor $\boldsymbol{\sigma}$ must also satisfy the balance equation of angular momentum, which turns out to be fulfilled if $\boldsymbol{\sigma}$ is symmetric

$$\boldsymbol{\sigma} = \boldsymbol{\sigma}^t. \tag{2}$$

Across the boundary $\partial\mathcal{B}_t$ of the body, the Cauchy stress tensor must satisfied the jump condition

$$[\![\boldsymbol{\sigma}]\!] \cdot \boldsymbol{n} = \boldsymbol{t}_t^m, \tag{3}$$

where $\boldsymbol{t}_t^m$ is the mechanical traction on $\partial\mathcal{B}_t$, $\boldsymbol{n}$ is the outward pointing unit normal to the boundary $\mathcal{B}_t$ and $[\![\bullet]\!] = [\bullet]_{inside} - [\bullet]_{outside}$. Note that under a normal mechanical loading this jump condition reduces to

$$\boldsymbol{\sigma} \cdot \boldsymbol{n} = \boldsymbol{t}_t^m, \tag{4}$$

since the Cauchy stress tensor vanishes identically outside the material body.

In order to formulate a variational equation for the problem we assume that there exists a stored energy density function $W_{0\boldsymbol{F}} = W_{0\boldsymbol{F}}(\boldsymbol{F})$ per unit volume of the undeformed configuration $\mathcal{B}_0$ so that the Cauchy stress tensor $\boldsymbol{\sigma}$ can be computed by

$$\boldsymbol{\sigma} = J^{-1}\boldsymbol{F} \cdot \partial_{\boldsymbol{F}} W_{0\boldsymbol{F}}^t, \tag{5}$$

where $J = \det \boldsymbol{F}$. In this case in reference to the deformed configuration $\mathcal{B}_t$ the problem of nonlinear elastostatics can be formulated in the variational format

$$\delta \int_{\mathcal{B}_t} W_{t\boldsymbol{F}} dv - \int_{\mathcal{B}_t} \boldsymbol{b}_t \cdot \delta\boldsymbol{\varphi} dv - \int_{\partial\mathcal{B}_t} \boldsymbol{t}_t^m \cdot \delta\boldsymbol{\varphi} ds = 0, \tag{6}$$

where $W_{t\boldsymbol{F}} = J^{-1}W_{0\boldsymbol{F}}$ is the stored energy density per unit volume of the deformed configuration $\mathcal{B}_t$.

## 3. Governing equations of nonlinear electro-elastostatics

When a polarizable body is immersed in an electric field, the body deforms because of the electric body force that the electric field exerts on the material. At every point inside the body, this electric body force depends on the electric field and the polarization. The electric field is governed by the four Maxwell's equations. In reference to the deformed configuration $\mathcal{B}_t$, the first Maxwell's equation, i.e. the Gauss' law, is written in terms of free charges as

$$\nabla_{\boldsymbol{x}} \cdot \mathbb{d} = \varrho_t^f, \tag{7}$$

where $\mathbb{d}$ is the electric displacement and $\varrho_t^f$ is the density of free charges. For the sake of simplicity we will assume that free charges exist only on the boundary surface $\partial\mathcal{B}_t$ of the body so that in the above equation $\varrho_t^f = 0$. We bypass the second and the fourth Maxwell's equations (Gauss' law for magnetism and Ampere's law) because of the assumption that there exist no magnetic field and no electric current. The third Maxwell's equation or the Faraday's law of induction is written here in the format

$$\nabla_{\boldsymbol{x}} \times \mathbb{e} = \boldsymbol{0}, \tag{8}$$

where $\mathbb{e}$ is the electric field. Across the boundary $\partial\mathcal{B}_t$, the electric field $\mathbb{e}$ and the electric displacement $\mathbb{d}$ must satisfy the jump conditions

$$\boldsymbol{n} \times [\![\mathbb{e}]\!] = \boldsymbol{0} \quad \text{and} \quad \boldsymbol{n} \cdot [\![\mathbb{d}]\!] = -\hat{\varrho}_t^f, \tag{9}$$

where $\hat{\varrho}_t^f$ is the surface free charge density on $\partial\mathcal{B}_t$. More details about governing equations of electric fields can be found, for example, in [17–20].

Also in reference to the deformed configuration $\mathcal{B}_t$, the electric body force can be computed as

$$\boldsymbol{b}_t^e = [\nabla_{\boldsymbol{x}}\mathbb{e}] \cdot \mathbb{p}, \tag{10}$$

where $\mathbb{p}$ is the electric polarization

$$\mathbb{p} = \mathbb{d} - \epsilon_0 \mathbb{e}. \tag{11}$$

With the help of Eqs. (7) and (8) the electric body force can be reformulated in the format

$$\boldsymbol{b}_t^e = \nabla_{\boldsymbol{x}} \cdot \left[\mathbb{e} \otimes \mathbb{d} - \frac{1}{2}\epsilon_0[\mathbb{e} \cdot \mathbb{e}]\boldsymbol{I}\right], \tag{12}$$

where $\boldsymbol{I}$ is the second order identity tensor and $\otimes$ represents the dyadic product.

With the electric body force $\boldsymbol{b}_t^e$, the balance equation of linear momentum reads

$$\nabla_{\boldsymbol{x}} \cdot \boldsymbol{\sigma}^t + \boldsymbol{b}_t + \boldsymbol{b}_t^e = \boldsymbol{0}. \tag{13}$$

By using the balance equation of angular momentum it can be shown that because of the electric body force, the Cauchy stress tensor $\boldsymbol{\sigma}$ is not symmetric in this case. However, if by using Eq. (12) we define a total stress tensor $\hat{\boldsymbol{\sigma}}$ as

$$\hat{\boldsymbol{\sigma}} = \boldsymbol{\sigma} + \mathbb{d} \otimes \mathbb{e} - \frac{1}{2}\epsilon_0[\mathbb{e} \cdot \mathbb{e}]\boldsymbol{I}, \tag{14}$$

then this total stress tensor turns out to be symmetric.

Across the boundary $\partial\mathcal{B}_t$, the jump condition for the stress can be written in terms of the total stress tensor $\hat{\boldsymbol{\sigma}}$ as

$$[\![\hat{\boldsymbol{\sigma}}]\!] \cdot \boldsymbol{n} = \boldsymbol{t}_t^m, \tag{15}$$

where $\boldsymbol{t}_t^m$ is again the mechanical surface traction in (3). For further discussions about the jump condition for the total stress tensor, see for example [21].

In summary, the governing equations above can be rewritten as

$$\begin{cases} \nabla_{\boldsymbol{x}} \cdot \hat{\boldsymbol{\sigma}}^t + \boldsymbol{b}_t = \boldsymbol{0} \quad \text{and} \quad \nabla_{\boldsymbol{x}} \cdot \mathbb{d} = 0 \quad \text{in} \quad \mathcal{B}_t, \\ \hat{\boldsymbol{\sigma}} \cdot \boldsymbol{n} = \bar{\boldsymbol{t}}_t \quad \text{and} \quad \mathbb{d} \cdot \boldsymbol{n} = -\bar{q}_t \quad \text{on} \quad \partial\mathcal{B}_t \end{cases} \tag{16}$$

in reference to the deformed configuration $\mathcal{B}_t$. In the above system, the stress tensor $\hat{\boldsymbol{\sigma}}$ and the electric displacement vector $\mathbb{d}$ are computed inside the body, whereas the traction $\bar{\boldsymbol{t}}_t$ and the electric surface flux $\bar{q}_t$ are computed by taking into account the contribution of the free space

$$\bar{\boldsymbol{t}}_t = \boldsymbol{t}_t^m + \hat{\boldsymbol{\sigma}}^{\epsilon_0} \cdot \boldsymbol{n}, \tag{17}$$

$$\bar{q}_t = -\mathbb{d}^{\epsilon_0} \cdot \boldsymbol{n} + \hat{\varrho}_t^f, \tag{18}$$

where we denote the quantities in the free space outside the body using the superscript $^{\epsilon_0}$.

In order to formulate a variational equation for the problem of nonlinear electro-elastostatics, let us assume that there exist some stored energy density functions $W_{0\mathbb{e}} = W_{0\mathbb{e}}(\boldsymbol{F}, \mathbb{e})$ and $W_{0\mathbb{E}} = W_{0\mathbb{E}}(\boldsymbol{F}, \mathbb{E})$ per unit volume of the undeformed configuration such that $W_{0\mathbb{e}}|_{\boldsymbol{F},\mathbb{e}} = W_{0\mathbb{E}}|_{\boldsymbol{F},\mathbb{E}}\ \forall \boldsymbol{F}, \mathbb{E}$ and that the Cauchy stress tensor $\boldsymbol{\sigma}$ and the electric polarization $\mathbb{p}$ can be computed by

$$\boldsymbol{\sigma} = J^{-1}\boldsymbol{F} \cdot [\partial_{\boldsymbol{F}} W_{0\mathbb{e}}]^t \quad \text{and} \quad \mathbb{p} = -J^{-1}\partial_{\mathbb{e}} W_{0\mathbb{e}}. \tag{19}$$

With this assumption in reference to the deformed configuration $\mathcal{B}_t$, the electric displacement $\mathbb{d}$ and the total stress tensor can be calculated as

$$\mathbb{d} = -J^{-1}\boldsymbol{F} \cdot \partial_{\mathbb{E}} \widehat{W}_{0\boldsymbol{F}} \tag{20}$$

and

$$\hat{\boldsymbol{\sigma}} = J^{-1}\boldsymbol{F} \cdot [\partial_{\boldsymbol{F}} \widehat{W}_{0\boldsymbol{F}}]^t, \tag{21}$$

where the stored energy density function $\widehat{W}_{0\boldsymbol{F}}$ is defined as the combination of the contributions of matter and free space

$$\widehat{W}_{0\boldsymbol{F}} = W_{0\mathbb{E}}(\boldsymbol{F},\mathbb{E}) - \frac{1}{2}\epsilon_0 J\boldsymbol{C}^{-1} : [\mathbb{E}\otimes\mathbb{E}]. \tag{22}$$

By using Eq. (19)–(22), the variational statement of the problem can eventually be formulated as

$$\delta\int_{\mathcal{B}_t}\widehat{W}_{t\boldsymbol{F}}dv - \int_{\mathcal{B}_t}\boldsymbol{b}_t\cdot\delta\boldsymbol{\varphi}dv - \int_{\partial\mathcal{B}_t}\bar{\boldsymbol{t}}_t\cdot\delta\boldsymbol{\varphi}ds + \int_{\partial\mathcal{B}_t}\delta\psi\bar{q}_t ds = 0 \tag{23}$$

in reference to $\mathcal{B}_t$ where $\psi$ is some electric potential such that

$$\mathbb{e} = -\frac{\partial\psi}{\partial\boldsymbol{x}} \tag{24}$$

besides $\widehat{W}_{t\boldsymbol{F}} = J^{-1}\widehat{W}_{0\boldsymbol{F}}$.

## 4. Boundary integral equations for the free space

As mentioned above, the surface terms in the variational equation (23) are computed by using the contribution of the free space surrounding the body of interest. When this contribution is small and can be ignored, it is convenient to use the finite element method to discretize equation (23) and solve for the unknowns $\boldsymbol{\varphi}$ and $\psi$. In the case the contribution of the free space must be taken into account, the computation of the surface terms in (23) requires the knowledge of the electric field in the free space. In the numerical computation of the electric field in the free space surrounding a body, a large finite element mesh can be used with the assumption that at the boundary of this large mesh the electric flux is negligible. It is a rule of thumb that this finite element mesh should be about five times the size of the body itself [22]. This requirement seems to be not a serious obstacle given the power of computers today. However, this is only true if on the boundary $\partial\mathcal{B}_t$ the displacement is small. In the case of small displacements, the configuration of the free space can be considered as unchanged and no remesh is needed. In other cases a remesh is required after every few iterations, which becomes particularly costly in three dimensional computations. In this work, we use the boundary element method to treat the electric field in the free space. For this purpose, the governing equations of the electric field outside $\mathcal{B}_t$ is written as

$$\begin{cases} \nabla^2_{\boldsymbol{x}}\psi^{\epsilon_0} = 0 & \text{outside } \mathcal{B}_t,\\ \psi^{\epsilon_0} = \bar{\psi} & \text{on } \partial\mathcal{B}_t^{\psi},\\ \mathbb{d}^{\epsilon_0}\cdot\boldsymbol{n} = -q_t = -\bar{q}_t + \hat{\varrho}_t^f & \text{on } \partial\mathcal{B}_t^{q}, \end{cases} \tag{25}$$

where $\psi^{\epsilon_0}$ is the electric potential in the free space, $\partial\mathcal{B}_t = \partial\mathcal{B}_t^{\psi}\cup\partial\mathcal{B}_t^{q}$, $\emptyset = \partial\mathcal{B}_t^{\psi}\cap\partial\mathcal{B}_t^{q}$, $\partial\mathcal{B}_t^{\psi}$ is the part of $\partial\mathcal{B}_t$ on which the potential $\psi^{\epsilon_0}$ is prescribed and $\partial\mathcal{B}_t^{q}$ is the part of $\partial\mathcal{B}_t$ on which the surface charge $\hat{\varrho}_t^f$ is prescribed. Note that in the above system, the normal vector $\boldsymbol{n}$ points from the inside to the outside of the domain $\mathcal{B}_t$.

Let us suppose that the free space surrounding $\mathcal{B}_t$ has two parts (Fig. 1), a finite part $\mathcal{V}_t^f$ (cavity) and an infinite part $\mathcal{V}_t^i$ such that $\partial\mathcal{B}_t = \partial\mathcal{V}_t^f\cup\partial\mathcal{V}_t^i$, $\partial\mathcal{B}_t^{\psi} = \partial\mathcal{V}_t^{f\psi}\cup\partial\mathcal{V}_t^{i\psi}$, $\partial\mathcal{B}_t^{q} = \partial\mathcal{V}_t^{fq}\cup\partial\mathcal{V}_t^{iq}$. With the definitions of $\mathcal{V}_t^f$ and $\mathcal{V}_t^i$ as such, the system (25) can now be transformed into the following system of two boundary integral equations

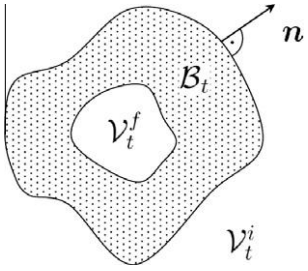


**Fig. 1.** Infinite ($\mathcal{V}_t^i$) and finite ($\mathcal{V}_t^f$) free space.

$$\int_{\partial\mathcal{V}_t^f}[\psi(\boldsymbol{x})-\psi(\boldsymbol{\xi})]\frac{\partial G(\boldsymbol{\xi},\boldsymbol{x})}{\partial n}ds - \int_{\partial\mathcal{V}_t^f}\frac{q_t}{\epsilon_0}G(\boldsymbol{\xi},\boldsymbol{x})ds = 0 \tag{26}$$

and

$$\psi(\boldsymbol{\xi}) - \psi_\infty - \int_{\partial\mathcal{V}_t^i}[\psi(\boldsymbol{x})-\psi(\boldsymbol{\xi})]\frac{\partial G(\boldsymbol{\xi},\boldsymbol{x})}{\partial n}ds + \int_{\partial\mathcal{V}_t^i}\frac{q_t}{\epsilon_0}G(\boldsymbol{\xi},\boldsymbol{x})ds = 0, \tag{27}$$

where $\psi_\infty$ is the electric potential at infinity, $\boldsymbol{x}$ is called the field point, $\boldsymbol{\xi}$ is the source point, $\frac{\partial[\bullet]}{\partial n}$ is the directional derivative along $\boldsymbol{n}$, $G(\boldsymbol{\xi},\boldsymbol{x})$ is the so-called fundamental solution and

$$q_t = \epsilon_0\frac{\partial\psi(\boldsymbol{x})}{\partial n} = -\epsilon_0\mathbb{e}^{\epsilon_0}\cdot\boldsymbol{n} = -\mathbb{d}^{\epsilon_0}\cdot\boldsymbol{n}. \tag{28}$$

In the above equation, the notation $\psi^{\epsilon_0}$ is replaced by $\psi$ due to the fact that the electric potential must be continuous across the boundary of the body. In addition, in three dimensional space the fundamental solution to the Laplace operator reads

$$G(\boldsymbol{\xi},\boldsymbol{x}) = \frac{1}{4\pi}\frac{1}{|\boldsymbol{\xi}-\boldsymbol{x}|}. \tag{29}$$

Besides equations (26) and (27), we assume that the total free charge in the system is zero. This condition can be expressed as

$$\int_{\mathcal{B}_t}\varrho_t^f dv + \int_{\partial\mathcal{B}_t}\hat{\varrho}_t^f ds = \int_{\partial\mathcal{B}_t}\left[\mathbb{d}\cdot\boldsymbol{n} + \hat{\varrho}_t^f\right]ds = -\int_{\partial\mathcal{B}_t}q_t ds = 0. \tag{30}$$

In what follows, we will use the boundary element method to discretize the boundary integral equations (26), (27) and (30). For more details about boundary integral equations and the theory of the boundary element method, see for example [23–25]. Note the difficulty in solving equations (26)–(29) due to the nonlinearity arising from the non constant integration domains resulting from the coupling with the nonlinearly deforming electroelastic body. Thus a Newton–Raphson scheme is needed even for the solution of the boundary integral equations.

## 5. Coupled BEM–FEM discretization

By viewing the above formulation, the problem of nonlinear electro-elastostatics can now be represented by the system of equations (23), (26), (27) and (30) with unknowns $\boldsymbol{\varphi}$, $\psi$ and $q_t$. Let us assume that the body is divided into *nel* domains or solid elements. Inside each solid element the displacement is approximated as

$$\boldsymbol{\varphi} = \sum_{k=1}^{nen}N^k\boldsymbol{\varphi}_k \tag{31}$$

and the electric potential is approximated as

$$\psi = \sum_{k=1}^{nen}N^k\psi_k, \tag{32}$$

where $N^k$ is the shape function at node $k$, *nen* is the number of nodes per element, $\boldsymbol{\varphi}_k$ is the displacement vector at node $k$ and $\psi_k$ is the electric potential at node $k$.

By using the above approximations, the variational statement (23) can be discretized in the format

$$\begin{aligned}&\sum_{e=1}^{nel}\sum_{k=1}^{nen}\left[\delta\boldsymbol{\varphi}_k\cdot\int_{\mathcal{B}_t^e}\hat{\boldsymbol{\sigma}}\cdot\nabla_{\boldsymbol{x}}N^k dv + \delta\psi_k\int_{\mathcal{B}_t^e}\mathbb{d}\cdot\nabla_{\boldsymbol{x}}N^k dv\right]\\ &\quad-\sum_{e=1}^{nel}\sum_{k=1}^{nen}\left[\delta\boldsymbol{\varphi}_k\cdot\int_{\mathcal{B}_t^e}\boldsymbol{b}_t N^k dv + \delta\boldsymbol{\varphi}_k\cdot\int_{\partial\mathcal{B}_t^e}\bar{\boldsymbol{t}}_t N^k ds - \delta\psi_k\int_{\partial\mathcal{B}_t^e}\bar{q}_t N^k ds\right]\\ &\quad=0,\end{aligned} \tag{33}$$

where $\mathcal{B}_t^e$ is the space occupied by element $e$. Note that at the boundary of the body besides the mechanical traction $\boldsymbol{t}_t^m$, the elec-

tric contribution of the free space to the surface traction $\bar{\boldsymbol{t}}_t$ is the surface traction due to the Maxwell's stress

$$\boldsymbol{t}_t^e = \epsilon_0[\mathbb{e}\otimes\mathbb{e}]\cdot\boldsymbol{n} - \frac{1}{2}\epsilon_0[\mathbb{e}\cdot\mathbb{e}]\boldsymbol{n} \tag{34}$$

and thus we have $\bar{\boldsymbol{t}}_t = \boldsymbol{t}_t^m + \boldsymbol{t}_t^e$. In order to compute the traction $\boldsymbol{t}_t^e$, we rewrite the electric field vector in the format

$$\mathbb{e} = \mathbb{e}_t + \mathbb{e}_n, \tag{35}$$

where $\mathbb{e}_n$ is the normal part of $\mathbb{e}$

$$\mathbb{e}_n = [\mathbb{e}\cdot\boldsymbol{n}]\boldsymbol{n} \tag{36}$$

and $\mathbb{e}_t$ is the tangential part of $\mathbb{e}$. The normal part of $\mathbb{e}$ is computed by using the electric flux on the boundary of the body. By using the decomposition (35), the electric traction $\boldsymbol{t}_t^e$ can now be written as

$$\boldsymbol{t}_t^e = \frac{1}{2\epsilon_0}q_t^2\boldsymbol{n} - q_t\mathbb{e}_t - \frac{1}{2}\epsilon_0[\mathbb{e}_t\cdot\mathbb{e}_t]\boldsymbol{n}. \tag{37}$$

In the above equation $q_t$ is the flux defined in (28) that will be computed using the help of the boundary integral equations (26), (27), and (30). In order to discretize these equations, let us assume that the surface $\partial\mathcal{B}_t$ is discretized using surface elements whose nodes coincide with that of solid elements used to discretized $\mathcal{B}_t$. The displacement over a particular surface element $e$ is approximated as:

$$\boldsymbol{\varphi} = \sum_{k=1}^{nens} N_s^k\boldsymbol{\varphi}_k, \tag{38}$$

where *nens* is the number of nodes of the surface element $e$ that covers the surface $\partial\mathcal{B}_t^e$, $N_s^k$ is the shape function at node $k$ of the surface element $e$: $N_s^k = N_s^k(\xi,\eta)$. Also over this surface element, the electric potential is approximated in the same way as the displacement

$$\psi = \sum_{k=1}^{nens} N_s^k\psi_k. \tag{39}$$

At every point on $\partial\mathcal{B}_t^e$, the normal vector $\boldsymbol{n}$ is computed as

$$\boldsymbol{n} = \hat{\boldsymbol{g}}_1\times\hat{\boldsymbol{g}}_2, \tag{40}$$

where $\hat{\boldsymbol{g}}_1$ and $\hat{\boldsymbol{g}}_2$ are the two basis vectors defined by

$$\hat{\boldsymbol{g}}_1 = \frac{\boldsymbol{g}_1}{|\boldsymbol{g}_1|}, \quad \boldsymbol{g}_1 = \sum_{k=1}^{nens}\boldsymbol{\varphi}_k\frac{\partial N_s^k}{\partial\xi}, \tag{41}$$

$$\hat{\boldsymbol{g}}_2 = \frac{\boldsymbol{g}_2}{|\boldsymbol{g}_2|}, \quad \boldsymbol{g}_2 = \sum_{k=1}^{nens}\boldsymbol{\varphi}_k\frac{\partial N_s^k}{\partial\eta}. \tag{42}$$

By using (41) and (42) the tangential part $\mathbb{e}_t$ can be further decomposed into

$$\mathbb{e}_t = [\mathbb{e}\cdot\hat{\boldsymbol{g}}_1]\hat{\boldsymbol{g}}_1 + [\mathbb{e}\cdot\hat{\boldsymbol{g}}_2]\hat{\boldsymbol{g}}_2 \tag{43}$$

or with the help of the approximations (38) and (39)

$$\mathbb{e}_t = -\sum_{k=1}^{nens}\psi_k\frac{\partial N_s^k}{\partial\xi}\frac{\hat{\boldsymbol{g}}_1}{|\boldsymbol{g}_1|} - \sum_{k=1}^{nens}\psi_k\frac{\partial N_s^k}{\partial\eta}\frac{\hat{\boldsymbol{g}}_2}{|\boldsymbol{g}_2|}. \tag{44}$$

Note that the decomposition of the electric vector as presented above can be seen as a presentation of $\mathbb{e}$ in a coordinate system whose basis vectors are $[\hat{\boldsymbol{g}}_1,\hat{\boldsymbol{g}}_2,\hat{\boldsymbol{g}}_3]$ with $\hat{\boldsymbol{g}}_3 = \boldsymbol{n}$ and therefore

$$\mathbb{e} = e_1\hat{\boldsymbol{g}}_1 + e_2\hat{\boldsymbol{g}}_2 + e_3\hat{\boldsymbol{g}}_3, \tag{45}$$

where $e_1 = \mathbb{e}\cdot\hat{\boldsymbol{g}}_1$, $e_2 = \mathbb{e}\cdot\hat{\boldsymbol{g}}_2$, $e_3 = \mathbb{e}\cdot\hat{\boldsymbol{g}}_3$.

For simplicity, let us assume that the discretization of the boundary integral equations is realized using 4 node quadrilateral surface elements. The flux over each element is assumed to be constant and one source point is placed at the center of each surface element. Because the two boundary integral equations (26) and (27) are similar, let us consider only the discretization of (27), which reads

$$\sum_{j=1,j\in i}^{nens} N_s^j\psi_j - \psi_\infty + \sum_{e=1}^{nels}\int_{\partial\mathcal{B}_t^e}\frac{1}{4\pi}\frac{\boldsymbol{r}\cdot\boldsymbol{n}}{[\boldsymbol{r}\cdot\boldsymbol{r}]^{3/2}}\left[\sum_{k=1,k\in e}^{nens} N_s^k\psi_k - \sum_{j=1,j\in i}^{nens} N_s^j\psi_j\right]ds + \sum_{e=1}^{nels}\int_{\partial\mathcal{B}_t^e}\frac{1}{4\pi\epsilon_0}\frac{1}{[\boldsymbol{r}\cdot\boldsymbol{r}]^{1/2}}q_t^e ds = 0 \quad \forall i = \overline{1,nels}, \tag{46}$$

where $\boldsymbol{r} = \boldsymbol{x} - \boldsymbol{\xi}$, $\sum_{j=1,j\in i}^{nens} N_s^j\psi_j$ is the approximation of the electric potential at the source point $\boldsymbol{\xi}$ on the source element $i$, *nels* is the number of surface elements, $\sum_{k=1,k\in e}^{nens} N_s^k\psi_k$ is the approximation of the electric potential at the field point $\boldsymbol{x}$ on the field element $e$ and $q_t^e$ is the electric flux over $\partial\mathcal{B}_t^e$.

With the assumption that the electric flux over $\partial\mathcal{B}_t^e$ is constant, the total charge equation (30) is discretized as

$$\sum_{e=1}^{nels}\int_{\partial\mathcal{B}_t^e} q_t^e ds = 0. \tag{47}$$

Equations (33), (46) and (47) form a coupled BEM–FEM system of equations with nodal unknowns of the motion map $\boldsymbol{\varphi}$, the electric potential $\psi$ and the electric flux $q_t$. This system of equations is solved in this work by using the Newton–Raphson scheme, in which the very first step is to linearize equations (33), (46) and (47). In order to save space, the details of the linearization will not be presented there. For more details on linearization of the equation (33) using the finite element method, the readers are referred to, for example, the work of Wood and Bonet [26]. A frame work for the linearization of equations (46) and (47) using the boundary element method is detailed in the work of Steinmann [16].

## 6. Numerical studies

The main objective of our numerical studies is to compute the electric field and the deformation field inside a material body un-

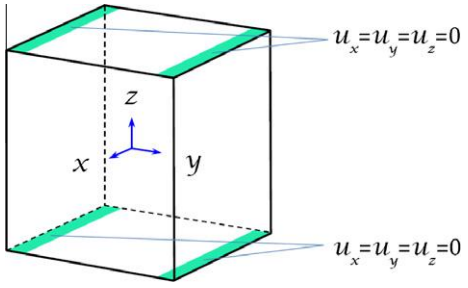


**Fig. 2.** Geometry, coordinate system and boundary conditions of the material body.

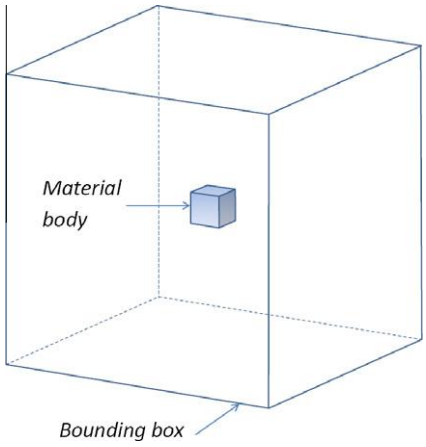


**Fig. 3.** Geometry of the material body and bounding box.

der electric loading and explore the influence of the surrounding free space. For this purpose, we consider here the simulation of a cube (the material body) with dimensions 60 μm × 60 μm × 60 μm (Fig. 2). The origin of the coordinate system is assumed to be at the center of the cube. On the lower ($z = -30$ μm) and upper ($z = +30$ μm) surfaces of the cube, the displacement is prescribed as (Fig. 2):

$$u_x = u_y = u_z = 0 \text{ for } -30\ \mu\text{m} \leqslant y \leqslant -24\ \mu\text{m and for } 24\ \mu\text{m} \leqslant y \leqslant 30\ \mu\text{m}. \tag{48}$$

The electric loading is applied on the body by mean of prescribed electric potentials ($\psi_{lower}$ and $\psi_{upper}$) given on the lower and upper surfaces of the cube. For the purpose of demonstration, the material properties are given through the stored energy density function $\widehat{W}_{0\mathbf{F}}$ defined here in the following format:

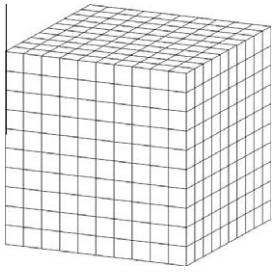

**Fig. 4.** Finite element mesh for the material body.

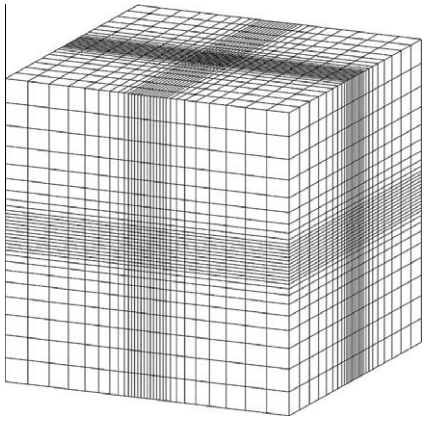

**Fig. 5.** Finite element mesh for the free space.

$$\widehat{W}_{0\mathbf{F}} = \frac{\mu}{2}[\boldsymbol{C} : \boldsymbol{I} - 3] - \mu \ln J + \frac{\lambda}{2}[\ln J]^2 + \alpha \boldsymbol{I} : [\mathbb{E} \otimes \mathbb{E}] + \beta \boldsymbol{C} : [\mathbb{E} \otimes \mathbb{E}] - \frac{1}{2}\epsilon_1 J \boldsymbol{C}^{-1} : [\mathbb{E} \otimes \mathbb{E}], \tag{49}$$

where $\mu = 0.05$ MPa, $\lambda = 0.06$ MPa, $\alpha = 0.2\epsilon_0$, $\beta = 2\epsilon_0$, $\epsilon_1 = 5\epsilon_0$ and $\epsilon_0 = 8.854 \times 10^{-12}$ F/m.

In what follows, we consider three numerical studies: (1) moderate electric loading, (2) high electric loading and (3) convergence property. In the first study, the cube is loaded with relative small values of $\psi_{lower}$ and $\psi_{upper}$. In the second study, the cube is loaded with some higher values of $\psi_{lower}$ and $\psi_{upper}$. In the third study, we examine the convergence property of the coupled BEM–FEM approach presented above.

### 6.1. Moderate electric loading

For this case, the electric loading is given by prescribing $\psi_{lower} = -100$ V and $\psi_{upper} = +100$ V. Three different approaches are used here to simulate the cube. The first approach is called FEM with truncation of free space. In this approach only the finite element method is used: both the cube and the free space surrounding the cube are modeled by finite elements. The free space is truncated by using a bounding box of the size 540 μm × 540 μm × 540 μm surrounding the cube (Fig. 3). Note that the size of the bounding box is 9 times the size of the cube in each direction. With this bounding box, the free space is now understood as the space between the boundary of the cube and the bounding box. On the boundary of this bounding box the electric flux can be considered to be negligible and the effect of the free space is accounted for with high accuracy. As consequence, the numerical solutions using this approach can be considered as accurate and will be used here to verify other simulation results.

In our simulation, the cube is simulated using a mesh that has 1000 solid 8-node hexagonal elements (Fig. 4) and the truncated free space is modeled using a mesh with 26,000 solid 8-node hexagonal elements (Fig. 5). For details of this approach see for example [22]. In the free space, only the information about the electric field is needed, therefore the nodal displacement of all finite element nodes lying outside the material body is prescribed as zero. Because the displacement of all nodes lying in the free space is prescribed as zero, the numerical simulation is only possible as long as elements lying next to the boundary of the cube remain not too much distorted. This means that in order to simulate large deformations, a remesh is required when distortion becomes a numerical problem. Despite the fact that a remesh is theoretically simple, the numerical implementation is still a work in progress. Therefore for the purpose of verifying other numerical results, the moderate electric loading with $\psi_{lower} = -100$ V and $\psi_{upper} = +100$ V is chosen

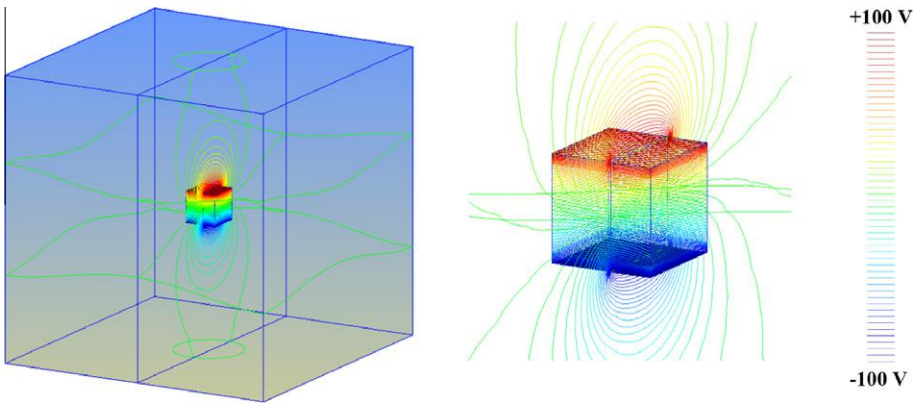


**Fig. 6.** Electric potential inside/ outside the material body (left) and close-up (right).

so that no remesh is needed. In the second approach the coupled BEM–FEM presented above is employed. In this approach, we use the same finite element mesh for the material body: the cube is modeled by 1000 solid 8-node hexagonal elements. However, the free space is taken into account with the help of 600 surface 4-node quadrilateral boundary elements that are attached to the boundary of the finite element mesh. In order to emphasize the effect of the energy stored in the free space on the deformation of the material body, the cube is simulated using a third approach in which only the cube is modeled using 1000 solid 8-node hexagonal elements and the free space is not taken into account. This approach is called here FEM without free space.

As numerical result, the electric potential computed by using the first approach is plotted in Fig. 6. A close-up is also presented in Fig. 6 to demonstrate the electric field near the boundary of the material body. It is easy to observe that the electric field outside the material body is considerably strong and therefore a considerable part of the energy is stored in the free space.

The displacement of the cube's edge with $x = 30$ μm, $z = 30$ μm computed using the three approaches is plotted in Fig. 7. It is observed that the result obtained by using the coupled BEM–FEM agrees very well with the one using the FEM with truncation of free space and that the influence of the free space on the simulated deformation is significant. For a better appreciation of this influ-

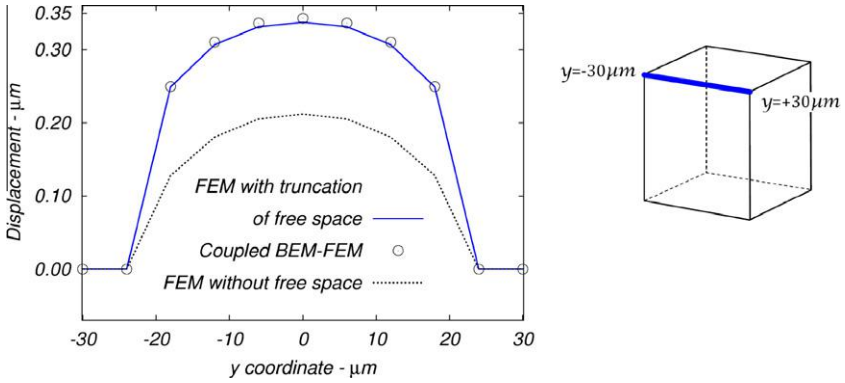


**Fig. 7.** Displacement under electric loading $\psi_{lower} = -100$ V and $\psi_{upper} = +100$ V.

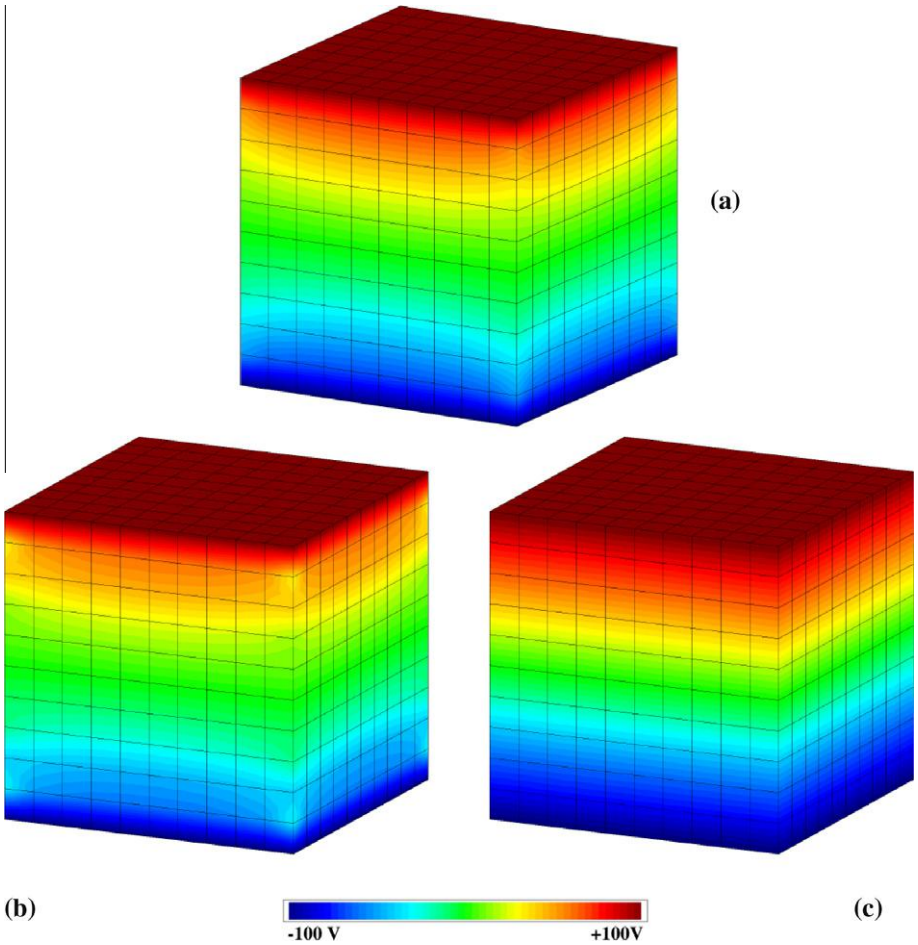


**Fig. 8.** Distribution of electric potential on undeformed configuration using: (a) FEM with truncation of free space, (b) coupled BEM–FEM and (c) FEM without free space.

ence, the distribution of the electric potential and the displacement of the cube computed by using the three approaches are presented in Figs. 8 and 9.

The numerical results show that the maximum displacement computed by using the first approach is 0.343 μm and by using the second approach is 0.337 μm. If the free space is not taken into account (FEM without free space), the maximum displacement is 0.212 μm, which is about 30% less than the case when the free space is taken into account.

### 6.2. High electric loading

For this case, the electric loading is given by prescribing $\psi_{lower} = -500$ V and $\psi_{upper} = +500$ V. In this case, because of large displacements at the boundary of the cube, the use of the FEM with truncation of free space will require a remesh of the free space. This, as mentioned above, is still a work in progress. Therefore only the coupled BEM–FEM and the FEM without free space are used to simulate the cube. The simulation using the coupled BEM–FEM

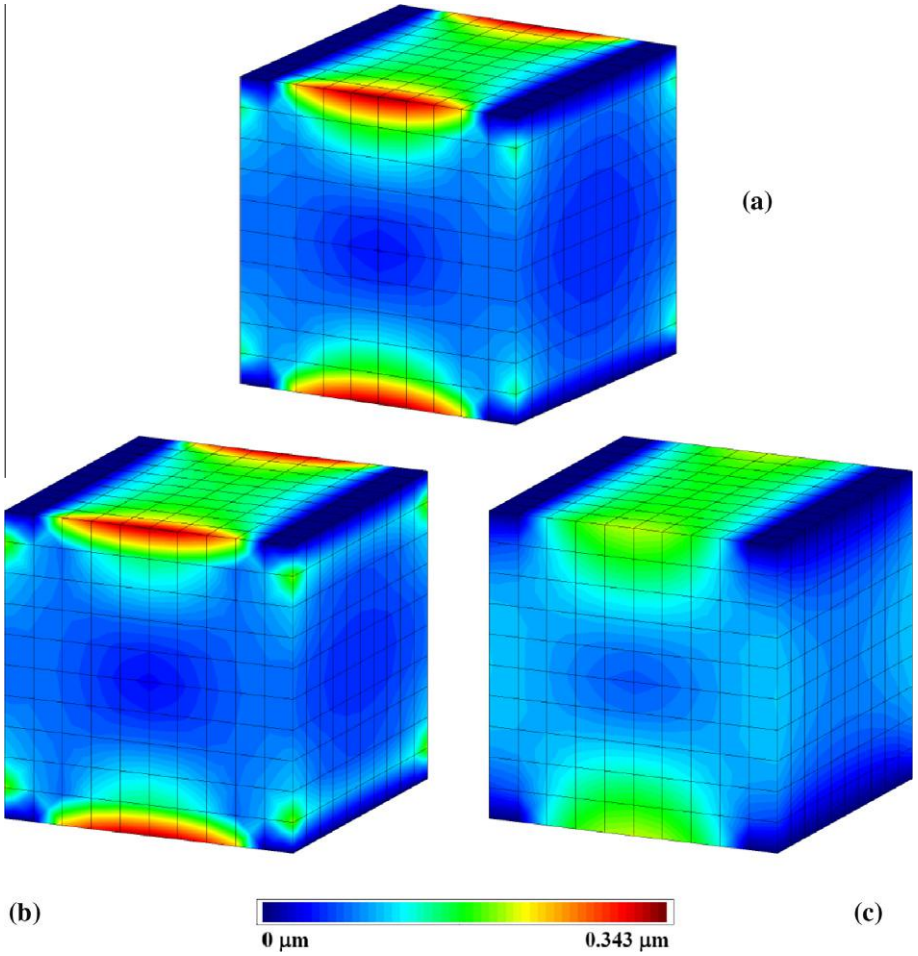


**Fig. 9.** Distribution of displacement on undeformed configuration under electric loading $\psi_{lower} = -100$ V and $\psi_{upper} = +100$ V using: (a) FEM with truncation of free space, (b) coupled BEM–FEM and (c) FEM without free space.

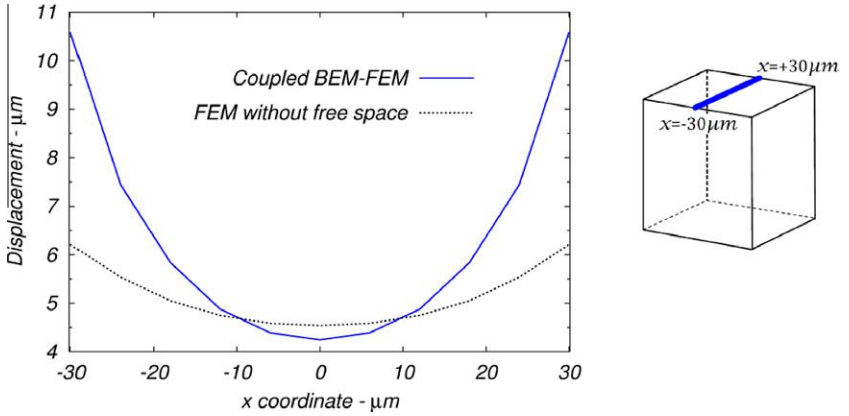


**Fig. 10.** Displacement under electric loading $\psi_{lower} = -500$ V and $\psi_{upper} = +500$ V.

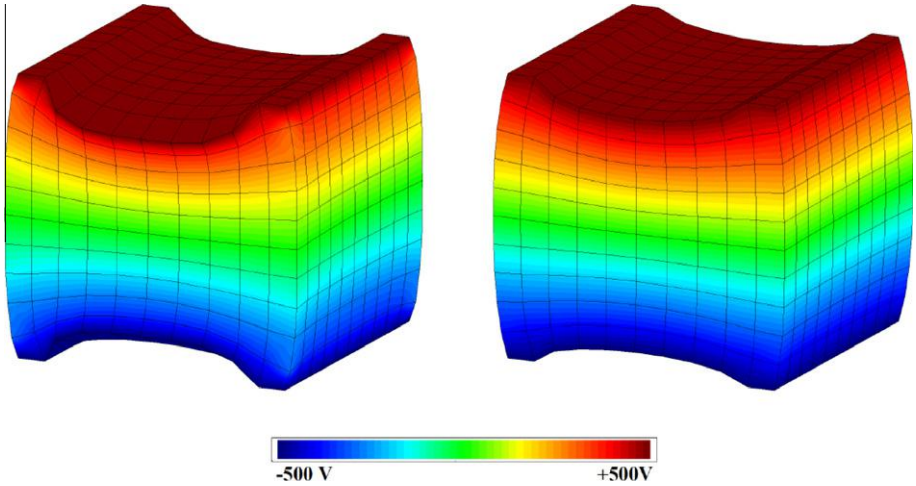


**Fig. 11.** Distribution of electric potential on deformed configuration using coupled BEM–FEM (left) and FEM without free space (right) under electric loading $\psi_{lower} = -500$ V and $\psi_{upper} = +500$ V.

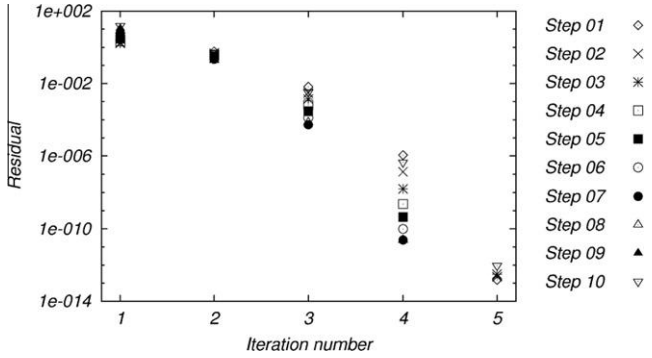


**Fig. 12.** Residual after each iteration.

gives maximum displacements of 10.591 μm whereas the result without the contribution of the free space is 6.209 μm. This difference can also be seen in Fig. 10 where the displacement of the line $y = 0$ μm, $z = 30$ μm is plotted. In Fig. 11 the distributions of the electric potential on the deformed configuration obtained by using the coupled BEM–FEM and by using the FEM without free space are presented where the difference in the distributions of the electric potentials and in the deformations can be seen.

### 6.3. Convergence property

In order to investigate the convergence property of the Newton–Raphson scheme used in the coupled BEM–FEM simulation, the loading $\psi_{lower} = -500$ V and $\psi_{upper} = +500$ V is applied in 10 steps. In each step the electric potential difference has an increment of 100 V and the numerical simulation is considered as converged when the residual of the system of equations (33), (46) and (47) is less than 1.0E−09. The residual after each iteration is presented in Fig. 12. It is observed that in each step only 4 or 5 iterations are needed to reach convergence. Besides, a quadratic convergence is also noted.

## 7. Conclusion

In this work the simulation of nonlinear electro-elastostatics is addressed with the main emphasis on the influence of the free space surrounding an electro-sensitive body. This influence becomes highly important, for example, in the case of EEAPs – the materials that are used in developing artificial muscles. In order to take into account the influence of the free space, we use a coupled BEM–FEM approach, in which the BEM is used to simulate the free space and the FEM is used to simulate the nonlinear body. The use of the BEM is a user-friendly approach because the BEM mesh needed in the simulation can be constructed automatically on the existing FEM mesh. The accuracy of the simulation using the coupled BEM–FEM is verified and its convergence rate is demonstrated to be satisfactory. Numerical results using the coupled BEM–FEM show that the contribution of the free space can alter profoundly the electric field and the deformation field inside a body made of materials with low electric permittivity like EEAPs. The use of the coupled BEM–FEM can therefore help improve the design of artificial muscles using EEAPs. Despite the fact that only the static case of electro-elasticity is considered in this work, the use of the coupled BEM–FEM is not limited to the simulation of nonlinear electro-elastostatics but can be extended to the general case of nonlinear electro-elasticity and nonlinear electro-viscoelasticity, which constitutes the direction for future works.

## Acknowledgments

The authors greatly acknowledge the financial support of the German Research Foundation (DFG) under the project "Electronic electroactive polymers under electric loading: Experiment, Modelling and Simulation", Grant No. STE 544/36-1.

## References

[1] Y. Bar-Cohen, Electro-active polymers: current capabilities and challenges, in: EAPAD Conference, San Diego, CA, March 18–21, 2002, paper 4695-02.
[2] Y. Bar-Cohen, Current and future developments in artificial muscles using electroactive polymers, Expert Rev. Med. Devices J. Future Drugs 1 (2005) 731–740.
[3] Y. Bar-Cohen, Artificial muscles using electroactive polymers, in: Y. Bar-Cohen (Ed.), Biomimetics: Biologically Inspired Technologies, Taylor and Francis, 2006.
[4] Y. Bar-Cohen, Biomimetics – using nature to inspire human innovation, Bioinspirat. Biomimet. 1 (2006) 1–12.
[5] Y. Bar-Cohen, Directions for development of the field of electroactive polymer, in: EAPAD Conference, San Diego, CA, March 28, 2011, paper 7976-04.
[6] R. Baumgartner, C. Keplinger, R. Kaltseis, R. Schwoediauer, S. Bauer, Dielectric elastomers: from the beginning of modern science to applications in actuators and energy harvesters, in: EAPAD Conference, San Diego, CA, March 28, 2011, paper 7976-03.
[7] D.M. Opris, M. Molberg, F. Nnesch, C. Lwe, C. Walder, B. Fischer, Dielectric elastomer materials for actuators and energy harvesting, in: EAPAD Conference, San Diego, CA, March 28, 2011, paper 7976-0G.

[8] M.G. Thomas, B.M. OBrien, E.P. Calius, I.A. Anderson, Soft generators using dielectric elastomers, Appl. Phys. Lett. 98 (2011). 142903-142903-3.
[9] D.K. Vu, P. Steinmann, G. Possart, Numerical modelling of nonlinear electroelasticity, Int. J. Numer. Methods Engrg. 70 (2006) 685–704.
[10] D.K. Vu, P. Steinmann, A 2-d coupled BEM-FEM simulation of electro-elastostatics at large strain, Comput. Methods Appl. Mech. Engrg. 199 (2010) 1124–1133.
[11] G. Kofod, Dielectric elastomer actuators, Ph.D. thesis, The Technical University of Denmark, 2001.
[12] G. Kofod, P. Sommer-Larsen, Silicone dielectric elastomer actuators: finite elasticity model of actuation, Sens. Actuators A 122 (2005) 273–283.
[13] A. Dorfmann, R.W. Ogden, Nonlinear electroelasticity, Acta Mechanica 174 (2005) 167–183.
[14] G.A. Maugin, Continuum Mechanics of Electromagnetic Solids, North-Holland, Amsterdam, 1988.
[15] P.A. Voltairas, D.I. Fotiadis, C. Massalas, A theoretical study of the hyperelasticity of electro-gels, Proc. Royal Soc. Math. Phys. Engrg. Sci. 459 (2003) 2121–2130.
[16] P. Steinmann, Computational nonlinear electro-elasticity – getting started, in: R. Ogden, D. Steigmann (Eds.), Mechanics and Electrodynamics of Magneto- and Electro-elastic Materials (CISM International Centre for Mechanical Sciences), Springer, 2011.
[17] A.C. Eringen, G.A. Maugin, Electrodynamics of continua, Foundations and Solid Media, vol. 1, Springer-Verlag, New York, 1989.
[18] D.J. Griffiths, Introduction to Electrodynamics, Prentice Hall, 1998.
[19] A. Kovetz, Electromagnetic Theory, Oxford University Press, 2000.
[20] D.J. Steigmann, On the formulation of balance laws for electromagnetic continua, Math. Mech. Solids 14 (4) (2009) 390–402.
[21] R.M. McMeeking, C.M. Landis, Electrostatic forces and stored energy for deformable dielectric materials, Journal of Applied Mechanics – American Society Of Mechanical Engineers – ASME 72 (2005) 581–590.
[22] Q. Chen, A. Konrad, A review of finite element open boundary techniques for static and quasistatic electromagnetic field problems, IEEE Trans. Magnet. 33 (1997) 663–676.
[23] C. Brebbia, The Boundary Element Method for Engineers, Wiley, 1978.
[24] C.A. Brebbia, J.C.F. Telles, L.C. Wrobel, Boundary Element Techniques: Theory and Applications in Engineering, Springer, 1984.
[25] L.C. Wrobel, The Boundary Element Method, Application in Thermo-Fluids and Acoustics, vol. 1, Wiley, 2002.
[26] J. Bonet, R.D. Wood, Nonlinear Continuum Mechanics for Finite Element Analysis, Cambridge University Press, 1997.